

# Approximation of Reeb spaces with Mappers and Applications to Stochastic Filters

Mathieu Carrière\*, Bertrand Michel†

April 4, 2022

## Abstract

Reeb spaces, as well as their discretized versions called Mappers, are common descriptors used in Topological Data Analysis, with plenty of applications in various fields of science, such as computational biology and data visualization, among others. The stability and quantification of the rate of convergence of the Mapper to the Reeb space has been studied a lot in recent works [BBMW19, CMO18, CO17, MW16], focusing on the case where a scalar-valued filter is used for the computation of Mapper. On the other hand, much less is known in the multivariate case, where the domain of the filter is in  $\mathbb{R}^d$  instead of  $\mathbb{R}$ . The only available result in this setting [MW16] only works for topological spaces and cannot be used as is for finite metric spaces representing data, such as point clouds and distance matrices.

In this article, we present an approximation result for the Reeb space in the multivariate case using a Mapper-based estimator, which is a slight modification of the usual Mapper construction. Moreover, our approximation is stated with respect to a pseudometric that is an extension of the usual *interleaving distance* between persistence modules [CdSGO16]. Finally, we apply our results to the case where the filter function used to compute the Mapper is estimated from the data. We provide applications of this setting in statistics and machine learning and probability for different kinds of target filters, as well as numerical experiments that demonstrate the relevance of our approach.

## 1 Introduction

The *Reeb space* and the *Mapper* are common descriptors of Topological Data Analysis, that can summarize and encode the topological features of a given dataset using a continuous function, often called *filter*, defined on it. As such, both objects have been used tremendously in many different fields and applications of data science, including, among others, computational biology [CR19, JCR<sup>+</sup>19, NLC11, RCK<sup>+</sup>17], computer graphics [GSBW11, SMC07], or machine learning [BGC18, NLSKK18], and the Mapper has become the core product of the company Ayasdi<sup>1</sup>. Mathematically speaking, the Reeb space is a quotient space and the Mapper is a simplicial complex. Both objects are representatives of the topology of the input dataset, in the sense that any topological feature that is present in these objects witnesses the presence of an equivalent one in the input data. Moreover, the Mapper can be thought of as a more tractable approximation of the Reeb space, which, as a quotient space, might be difficult to describe and compute exactly. In the simpler case where the filter function is scalar-valued, the Mapper and the Reeb space actually become combinatorial graphs, which is why they are mostly used for clustering and visualizing data. Actually, even when the filter is multivariate, i.e., when its domain belongs to  $\mathbb{R}^d$  with  $d > 1$ , it is common to only compute the skeleton in dimension 1 of the Mapper, so as to make it easy to display and interpret.

In recent works, different notions of stability and convergence of the Mapper to the Reeb space, in the case where the filter function is scalar-valued, have been defined and studied [BGW14, BBMW19, CMO18, CO17, dSMP16], under various statistical assumptions on how data is generated. The more general case of multivariate filter functions is however much more difficult and less understood, since the singular values of the filter function, which turn out to be critical quantities to look at in the analysis, cannot be ordered easily,

\*Department of Systems Biology, Columbia University, United States, mc4660@cumc.columbia.edu

†Laboratoire de Mathématiques Jean Leray UMR.C 6629, Ecole Centrale de Nantes, France, bertrand.michel@ec-nantes.fr

<sup>1</sup>See <https://www.ayasdi.com/>

and as a consequence, the natural stratification of data (that could be derived for scalar-valued functions) does not extend. The only available result, presented in [MW16], proves an nice approximation result for continuous spaces, but unfortunately does not apply when data is given as a finite metric space, such as a point cloud or a distance matrix.

Moreover, many of previously cited works only consider the case where the values of the Reeb filter (either scalar-valued or multivariate) are known exactly on the data points. This will not be the case if the filter function is estimated from the data, and thus different from the filter function used to compute the target Reeb space. This happens tremendously in statistics and machine learning, where the underlying filter is usually a predictor, that has to be estimated with standard machine learning methods. As explained in this paper, another interesting example is when the interesting and underlying filter is given by the (scalar-valued) means, or the (multivariate) histograms, of some conditional probability distributions associated to each point in the dataset, and that what is given at hand are merely single realizations of these distributions. Then, the usual way of computing Mappers will clearly not work, especially if these conditional probability distributions have large variances, since single realizations are not representative at all of the means, or histograms, of the conditional probability distributions.

**Contributions.** The contribution of this article is two-fold:

- We first propose an approximation result, Theorem 3.3, of the Reeb space with a Mapper-based estimator in the general multivariate case. For this, we use a pseudometric which is a slight extension of the usual interleaving distance between persistence modules [CdSGO16].
- We then use this result in the so-called *Stochastic Filter* setting, where the filter used to compute the Mapper is only an estimation (usually computed from a random sample of data) of the target filter used to compute the corresponding Reeb space. We also provide applications and numerical experiments in statistics and machine learning, as well as examples in which the standard Mapper fails at recovering the correct topology of the data, while using our multivariate Mapper-based estimator succeeds at doing so.

The plan of this article is as follows: in Section 2, we recall the basics of Reeb spaces, Mappers, and we introduce our associated pseudometric. Then, we show our approximation result in Section 3, and we discuss the Stochastic Filter setting, with corresponding numerical experiments, in Section 4. Finally, we conclude and provide future investigations in Section 5.

## 2 Background on Reeb spaces and Mappers

In this section, we recall the definitions of the Reeb spaces and Mappers (Section 2.1), and we introduce the distance we use to compare them (Section 2.2).

### 2.1 Reeb spaces and Mappers

Reeb spaces and Mappers are mathematical constructions that enable to simplify and visualize the various topological structures that are present in topological spaces, through the lens of a continuous function, often called *filter*.

**Reeb space.** Given a topological space  $\mathcal{X}$  and a continuous function  $f : \mathcal{X} \rightarrow \mathbb{R}^d$ , the *Reeb space* of  $\mathcal{X}$  is an approximation of  $\mathcal{X}$  that preserves its connectivity structures. When  $f : \mathcal{X} \rightarrow \mathbb{R}$  is scalar-valued, it is usually called the *Reeb graph* [Ree46].

**Definition 2.1.** *Let  $\mathcal{X}$  be a topological space and  $f : \mathcal{X} \rightarrow \mathbb{R}^d$  be a continuous function defined on it. The Reeb space of  $\mathcal{X}$  is the quotient space:*

$$\mathbb{R}_f(\mathcal{X}) = \mathcal{X} / \sim_f,$$

where, for all  $x, x' \in \mathcal{X}$ , one has  $x \sim_f x'$  iff  $f(x) = f(x')$  and  $x, x'$  belong to the same connected component of  $f^{-1}(f(x)) = f^{-1}(f(y))$ .

**Approximation with Mapper.** However, the Reeb space is not well-defined when data is given as a finite metric space, i.e., a point cloud or a distance matrix, in which case all preimages used to compute the Reeb space are either empty or singletons. To handle this issue, the *Mapper* was introduced in [SMC07] as a tractable approximation of the Reeb space. We first provide its definition for continuous spaces.

**Definition 2.2.** Let  $\mathcal{X}$  be a topological space and  $f : \mathcal{X} \rightarrow \mathbb{R}^d$  be a continuous function defined on it. Moreover, let  $\mathcal{U}$  be a cover of  $\text{im}(f)$ , that is, a family of subsets  $\{U_\alpha\}_{\alpha \in A}$  of  $\mathbb{R}^d$  such that  $\text{im}(f) \subseteq \bigcup_{\alpha \in A} U_\alpha$ . Let  $\mathcal{V}$  be the cover of  $\mathcal{X}$  defined as  $\mathcal{V} = \{V \subseteq \mathcal{X} : \exists \alpha \in A \text{ s.t. } V \text{ is a connected component of } f^{-1}(U_\alpha)\}$ . The Mapper of  $\mathcal{X}, f, \mathcal{U}$  is then defined as:

$$M_{f, \mathcal{U}}(\mathcal{X}) = \mathcal{N}(\mathcal{V}),$$

where  $\mathcal{N}$  denotes the nerve of a cover.

**Parameters and extension to point cloud.** When data is given as a finite metric space, the connected components are usually identified with clustering, and the nerve is computed by assessing a non-empty intersection between several cover elements as soon as there exists at least one point that is shared by all these elements. In the remaining of this article, we use graph clustering. More precisely we assume that we have a graph  $G$  built on top of our finite metric space, and for each element  $U$  of the cover  $\mathcal{U}$ , we use the connected components of the subgraph  $G(U)$  to compute the Mapper. Here  $G(U)$  is defined as:

$$G(U) = (V_U, E_U), \tag{1}$$

where the vertex set  $V_U$  is  $\{v \in V(G) : f(v) \in U\}$  and the edge set  $E_U$  is  $\{(u, v) : u \in V_U, v \in V_U\}$ . When  $G$  is set to be the  $\delta$ -neighborhood graph  $G_\delta$ , this amounts to perform single-linkage clustering [MC12] with parameter  $\delta$ , and we let  $M_{f, \mathcal{U}, G_\delta}$  denote the corresponding Mapper for finite metric spaces.

Moreover, it is very usual to define a cover  $\mathcal{U}$  with hypercubes by covering every single dimension of  $\mathbb{R}^d$  with intervals of length  $r > 0$  and overlap percentage  $g \in [0, 1]$ , and then by taking the Euclidean products of these intervals. Note that  $r$  and  $g$  are often called the *resolution* and the *gain* of the cover respectively. We let  $\mathcal{U}(r, g)$  denote this particular type of cover. Note however that this strategy becomes quickly very expensive, and thus prohibitive, when the dimension  $d$  is large. Actually, even for moderate values, i.e.,  $d = 10$ , the computation can become very costly if the resolution is too small or the gain is too large. In Section 3, we provide alternative and computationally feasible strategies to cover the filter domain using thickenings of partitions.

It has been shown in recent works [BBMW19, CMO18, CO17, MW16] that the Mapper actually approximates the Reeb space under various assumptions and metrics when the filter is scalar-valued. In the next section, we introduce a new distance for multivariate Mappers and Reeb spaces, that we use to show a similar approximation result in Section 3.

## 2.2 The max-bottleneck distance

In this article, we compare Mappers and Reeb spaces with the *max-bottleneck distance*  $d_B^M$ , that we now introduce. Its definition is based on category theory and particular persistence modules that we call *anchored persistence modules*.

**Categories and Functors.** A *category* is an algebraic structure containing *objects* and *morphisms* or *arrows* between them. Among the various categories that have been defined in the literature, three are of particular interest in this article: the category **Open**( $\mathbb{R}^d$ ) of open sets in  $\mathbb{R}^d$ , where the morphisms are the inclusion maps  $U \rightarrow V \Leftrightarrow U \subseteq V$ , the category **Vect** of vector spaces with linear maps, and the category **Top** of topological spaces with continuous functions. A *functor* between two categories is a function  $F$  that maps any object (resp. morphism) of the first category, to an object (resp. morphism) of the second one. For instance, the *homology functor*  $H_*$  is a functor between **Top** and **Vect**. The max-bottleneck distance uses the following *functor representations* of Reeb spaces and Mappers, that are very similar (and were inspired from) the ones in [dSMP16, MW16].

**Definition 2.3.** The functor representation of a Reeb space  $R_f(\mathcal{X})$  is the functor  $F_{\mathcal{X},f} : \mathbf{Open}(\mathbb{R}^d) \rightarrow \mathbf{Vect}$ , which sends each object  $U \in \mathbb{R}^d$  to  $F_{\mathcal{X},f}(U) = H_0(f^{-1}(U))$ , and each morphism  $U \subseteq V$  to the morphism induced by the inclusion  $f^{-1}(U) \subseteq f^{-1}(V)$ .

Let  $\mathcal{U}$  be a cover of  $\text{im}(f)$ . Let  $\mathcal{N}(\mathcal{U})$  be the nerve of  $\mathcal{U}$ , and, for each  $\sigma = \{U_{\alpha_1}, \dots, U_{\alpha_p}\} \in \mathcal{N}(\mathcal{U})$ , let  $U_\sigma = \bigcap_{i=1}^p U_{\alpha_i}$ . The functor representation of the Mapper  $M_{f,\mathcal{U}}(\mathcal{X})$  is the functor  $F_{\mathcal{X},f,\mathcal{U}} : \mathbf{Open}(\mathbb{R}^d) \rightarrow \mathbf{Vect}$ , which sends each object  $U \in \mathbb{R}^d$  to  $F_{\mathcal{X},f,\mathcal{U}}(U) = H_0(f^{-1}(\bigcup_{\sigma \in K_U} U_\sigma))$ , where  $K_U = \{\sigma \in \mathcal{N}(\mathcal{U}) : U_\sigma \cap U \neq \emptyset\}$ , and each morphism  $U \subseteq V$  to the morphism induced by the inclusions  $K_U \subseteq K_V$  and  $f^{-1}(\bigcup_{\sigma \in K_U} U_\sigma) \subseteq f^{-1}(\bigcup_{\sigma \in K_V} U_\sigma)$ .

The max-bottleneck distance actually compares these functor representations by looking at their associated anchored persistence modules.

**Definition 2.4.** Let  $U$  be an open set of  $\mathbb{R}^d$ . The anchored persistence module associated to  $U$ , denoted by  $\Phi_{U,F}$ , is comprised of the indexed family of vector spaces  $\{F(U^\alpha)\}_{\alpha \geq 0}$ , where  $F$  is a functor between  $\mathbf{Open}(\mathbb{R}^d)$  and  $\mathbf{Vect}$  and  $U^\alpha$  is the  $\alpha$ -thickening of  $U$  defined with  $U^\alpha = \{x \in \mathbb{R}^d : \|x - U\| < \alpha\}$ , and of the doubly-indexed family of linear maps  $\{\phi_\alpha^\beta : F(U^\alpha) \rightarrow F(U^\beta)\}_{\alpha \leq \beta}$  induced by the inclusions  $U^\alpha \subseteq U^\beta$ .

Note that anchored persistence modules are persistence modules in the sense of [CdSGO16], that is, one has  $\phi_\alpha^\gamma = \phi_\beta^\gamma \circ \phi_\alpha^\beta$  for any  $\alpha \leq \beta \leq \gamma$ . The max-bottleneck distance looks at the possible interleavings between anchored persistence modules:

**Definition 2.5.** Let  $\epsilon > 0$ ,  $U$  be an open set of  $\mathbb{R}^d$  and  $\Phi_{U,F}$  and  $\Phi_{U,G}$  be the corresponding anchored persistence modules with functors  $F$  and  $G$ , and linear maps  $\phi_\alpha^\beta$  and  $\psi_\alpha^\beta$  respectively. One says that  $\Phi_{U,F}$  and  $\Phi_{U,G}$  are  $\epsilon$ -interleaved, if there exist linear maps  $a_\alpha : F(U^\alpha) \rightarrow G(U^{\alpha+\epsilon})$  and  $b_\alpha : G(U^\alpha) \rightarrow F(U^{\alpha+\epsilon})$  s.t. the following diagrams commute, for any  $\alpha \leq \beta$ :

$$\begin{array}{ccc}
F(U^\alpha) & \xrightarrow{\phi_\alpha^\beta} & F(U^\beta) & F(U^\alpha) & \xrightarrow{\phi_\alpha^{\alpha+2\epsilon}} & F(U^{\alpha+2\epsilon}) \\
\downarrow a_\alpha & & \downarrow a_\beta & \searrow a_\alpha & & \uparrow b_{\alpha+\epsilon} \\
G(U^{\alpha+\epsilon}) & \xrightarrow{\psi_{\alpha+\epsilon}^\beta} & G(U^{\beta+\epsilon}) & & & G(U^{\alpha+\epsilon}) \\
\\ 
G(U^\alpha) & \xrightarrow{\psi_\alpha^\beta} & G(U^\beta) & G(U^\alpha) & \xrightarrow{\psi_\alpha^{\alpha+2\epsilon}} & G(U^{\alpha+2\epsilon}) \\
\downarrow b_\alpha & & \downarrow b_\beta & \searrow b_\alpha & & \uparrow a_{\alpha+\epsilon} \\
F(U^{\alpha+\epsilon}) & \xrightarrow{\phi_{\alpha+\epsilon}^\beta} & F(U^{\beta+\epsilon}) & & & F(U^{\alpha+\epsilon})
\end{array}$$

Note that an interleaving is a notion that is well-defined for any pair of general persistence modules. The max-bottleneck distance is then simply defined as the smallest interleaving that is valid for any open set  $U$ :

**Definition 2.6.** Let  $\mathcal{X}$  be a topological space,  $f : \mathcal{X} \rightarrow \mathbb{R}^d$  be a continuous function and  $\mathcal{U}$  be a cover of  $\text{im}(f)$ . Let  $M_{f,\mathcal{U}}(\mathcal{X})$  and  $R_f(\mathcal{X})$  be the corresponding Mapper and Reeb space. The max-bottleneck distance  $d_B^M(M_{f,\mathcal{U}}(\mathcal{X}), R_f(\mathcal{X}))$  is defined as the smallest  $\epsilon > 0$  such that  $\Phi_{U,F_{\mathcal{X},f}}$  and  $\Phi_{U,F_{\mathcal{X},f,\mathcal{U}}}$  are  $\epsilon$ -interleaved for all  $U \in \mathbf{Open}(\mathbb{R}^d)$ .

The name bottleneck comes from the fact that interleaving distance between (tame) persistence modules was shown to be equal to the so-called *bottleneck distance* as defined in [CdSGO16]. Our distance can thus be thought of as an extension of the bottleneck distance between Mappers and Reeb graphs that was introduced in [CO17].

Note also that a distance between functor representations of Reeb spaces and Mappers, called the *interleaving distance* has already been introduced in [dSMP16] and [MW16]. This distance is stronger in the sense that it actually looks for interleavings between the functors themselves instead of their associated anchored persistence modules, and, as such, is always larger than the max-bottleneck distance (since any interleaving between the functors induces an interleaving between the modules). Moreover, since it was shown to satisfy an approximation property, this property directly extends to the max-bottleneck distance.

**Proposition 2.7** ([MW16]). Let  $\mathcal{X}$  be a topological space,  $f : \mathcal{X} \rightarrow \mathbb{R}^d$  be a continuous function and  $\mathcal{U}$  be a cover of  $\text{im}(f)$ . Moreover, let  $\text{res}(\mathcal{U}) = \max\{\text{diam}(U_\alpha) : U_\alpha \in \mathcal{U}\}$ . Then:

$$d_B^M(M_{f,\mathcal{U}}(\mathcal{X}), R_f(\mathcal{X})) \leq \text{res}(\mathcal{U})$$

Note however that these results only apply to topological spaces, and do not consider finite metric spaces, such as point clouds or distance matrices.

### 3 Reeb space approximation

In this section, we prove our approximation result Theorem 3.3 for our Mapper-based estimator. Since we hypothesize that our result holds when the domain of the target filter is a general metric space, we first generalize the Reeb space and the Mapper, and provide possible cover strategies, in Section 3.1. We then prove our approximation result in Section 3.2.

#### 3.1 Metric Reeb spaces and Mappers

Definitions 2.1 and 2.2 extend straightforwardly to the case where the domain of the filter  $f$  is a metric space  $\mathcal{S}$ . The only difference is in the definition of the Reeb space: the equivalence relation  $\sim_f$  becomes  $x \sim_f y$  iff  $d_{\mathcal{S}}(x, y) = 0$  and  $x, y$  belong to the same connected component of  $f^{-1}(f(x)) = f^{-1}(f(y))$ . In Section 4 below, we focus on two particular cases of interest: the first one is when  $\mathcal{S}$  is the space of probability distributions of  $\mathbb{R}$  (Section 4.2), and the second one is when  $\mathcal{S}$  is the space of combinatorial graphs (Section 4.3).

**Covers for metric spaces.** We now present a simple way of generating covers for a metric space from partitions of this space, by thickening the elements of the partition.

**Definition 3.1.** *Let  $(\mathcal{S}, d_{\mathcal{S}})$  be a metric space, and  $S \subseteq \mathcal{S}$  be a subset of  $\mathcal{S}$ . Let  $\epsilon > 0$ . The  $\epsilon$ -thickening of  $S$  is defined as  $S^\epsilon = \{s \in \mathcal{S} : \inf\{d_{\mathcal{S}}(s, \tilde{s}) : \tilde{s} \in S\} \leq \epsilon\}$ .*

*Now, let  $\mathcal{Q} = \{Q_\alpha\}_{\alpha \in A}$  be a partition of  $\mathcal{S}$ , i.e.,  $\mathcal{S} \subseteq \bigcup_{\alpha \in A} Q_\alpha$  and  $Q_\alpha \cap Q_\beta = \emptyset$  for all  $\alpha \neq \beta \in A$ . Let  $\epsilon > 0$ . The  $\epsilon$ -thickening of  $\mathcal{Q}$  is defined as  $\mathcal{Q}^\epsilon = \{Q_\alpha^\epsilon\}_{\alpha \in A}$ .*

Note that even when the filter is multivariate, that is, when  $\mathcal{S} = \mathbb{R}^d$ , it might be interesting to use thickenings of partitions instead of hypercube covers, since the number of hypercubes increases exponentially with the dimension  $d$ , with many of them having an empty preimage under  $f$ , and thus useless. On the other hand, partitions of  $\mathbb{R}^d$  can be computed very efficiently, for instance with Voronoi partitions or with the  $K$ -means algorithm.

#### 3.2 Reeb space approximation

In this section, we show that a multivariate Mapper-based estimator computed on a probabilistic sample can approximate the corresponding Reeb space under suitable statistical assumptions. Even though we restrict to the multivariate case, we hypothesize that the result holds in the more general case of filters with domains included in metric spaces (as described above in Section 3.1).

**Statistical setting.** In the remaining of this article, we use the same statistical setting of [CMO18]. More precisely, we let  $\hat{X}_n$  be a point cloud drawn from a probability measure  $P$  with the following assumptions:

- **Support.** The support  $\mathcal{X}$  of  $P$  is a compact submanifold  $\mathcal{X} \subseteq \mathbb{R}^D$  with positive convexity radius  $\rho = \rho(\mathcal{X})$ . Let  $D_{\mathcal{X}} < \infty$  denote the diameter of  $\mathcal{X}$ .
- **Measure.** The probability measure  $P$  is  $(a, b)$ -standard, i.e.,  $P(B(x, r)) \geq \min\{1, ar^b\}$ , for all  $x \in \mathcal{X}$  and  $r > 0$ , where  $B(x, r) = \{y \in \mathbb{R}^D : \|y - x\| \leq r\}$ .
- **Filter.** The filter  $f : \mathcal{X} \rightarrow \mathbb{R}^d$  has a modulus of continuity  $\omega$ , that is,  $\omega : \mathbb{R} \rightarrow \mathbb{R}$  is a continuous function such that  $\|f(x) - f(x')\| \leq \omega(\|x - x'\|)$ . Moreover, we assume that the filter values that we observe are from an estimation  $\hat{f}$  with modulus of continuity  $\hat{\omega}$ . Finally, let  $f_{\text{PL}}$  and  $\hat{f}_{\text{PL}}$  be the piecewise-linear extensions of  $f$  and  $\hat{f}$  on any geometric simplex whose vertices belong to  $\hat{X}_n$ .
- **Cover.** The cover  $\mathcal{U}$  is assumed to cover  $\text{im}(f) \cup \text{im}(f_{\text{PL}}) \cup \text{im}(\hat{f}) \cup \text{im}(\hat{f}_{\text{PL}})$ , and is supposed to be finite. Moreover, given a simplex  $\sigma = \{U_{\alpha_1}, \dots, U_{\alpha_p}\}$  in the nerve  $\mathcal{N}(\mathcal{U})$ , we let  $U_\sigma = \bigcap_{i=1}^p U_{\alpha_i}$ .

Finally, let  $s(n) = n/(\log n)^{1+\beta}$ , for some arbitrary  $\beta > 0$ ,  $\delta_n = d_H^E(\hat{X}_{s(n)}, \hat{X}_n)$  and  $\epsilon_n = d_H^E(\hat{X}_n, \mathcal{X})$ , where  $d_H^E$  is the Hausdorff distance computed with Euclidean distances.

**Proposed estimator.** We can now define our Mapper-based estimator. It is defined, for a random point cloud  $\hat{X}_n$  sampled from  $P$ , as a refinement of the standard multivariate Mapper. Let us first define the so-called *element-crossing edges*.

**Definition 3.2.** Let  $X_i, X_j \in \hat{X}_n$ , and let  $e = \{\alpha X_i + (1 - \alpha)X_j : \alpha \in [0, 1]\}$  be the segment obtained by interpolating linearly between these points. Note that  $\hat{f}_{\text{PL}}$  is well-defined on  $e$ . Hence, we say that  $e$  is an element-crossing edge if there exists  $\sigma \in \mathcal{N}(\mathcal{U})$  such that  $\hat{f}_{\text{PL}}(e) \cap U_\sigma \neq \emptyset$ ,  $\hat{f}_{\text{PL}}(X_i) \notin U_\sigma$  and  $\hat{f}_{\text{PL}}(X_j) \notin U_\sigma$ . In other words, the edge  $\hat{f}_{\text{PL}}(e)$  goes through  $U_\sigma$ , even though its endpoints  $\hat{f}_{\text{PL}}(X_i)$  and  $\hat{f}_{\text{PL}}(X_j)$  are outside  $U_\sigma$ . We say that  $U_\sigma$  is crossed by  $e$ .

Note that element-crossing edges are generalizations of *interval* and *intersection-crossing edges*, as defined in [CO17]. We can now define our estimator with the following steps.

- First, we define  $G_n = G_{\delta_n}$  as the neighborhood graph built on top of  $\hat{X}_n$  with parameter  $\delta_n$ , that is, any pair  $\{X_i, X_j\} \subset \hat{X}_n$  creates an edge in  $G_n$  iff  $\|X_i - X_j\| \leq \delta_n$ , and we let  $\hat{f}_{\text{PL}}(G_n)$  be the piecewise-linear metric embedding of  $G$  in the filter domain.
- Second, we define:

$$\ell(\hat{X}_n, \hat{f}, \mathcal{U}) = \inf\{|e \cap \mathcal{U}_\sigma| : e \text{ is element-crossing and } U_\sigma \text{ is crossed by } e\},$$

where  $|\cdot|$  denotes the length of an edge. In other words,  $\ell = \ell(\hat{X}_n, \hat{f}, \mathcal{U})$  is the length of the smallest intersection between an edge of  $\hat{f}_{\text{PL}}(G_n)$  and a cover element or intersection, such that the edge endpoints do not belong to this cover element or intersection.

- Finally, we let  $k_n$  be an arbitrary integer bigger than  $\lfloor \delta_n / \hat{\omega}^{-1}(\ell/2) \rfloor$  (we let  $k_n = +\infty$  if  $\ell = 0$ , which happens with null probability), and we subdivide each edge of  $G_n$  with  $k_n$  points. Moreover, we associate coordinates and filter values to these new interpolated points with  $\hat{f}_{\text{PL}}$ . Let  $\tilde{G}_n$  be the resulting graph, and  $\tilde{X}_n$  be the new point cloud.

Our estimator is then defined as:

$$M_n = M_{\hat{f}_{\text{PL}}, \mathcal{U}, \tilde{G}_n}(\tilde{X}_n) \quad (2)$$

Note that computing or estimating  $\ell(\hat{X}_n, \hat{f}, \mathcal{U})$  for a general cover  $\mathcal{U}$  is difficult, even though it can be done exactly for particular covers, such the ones induced by thickening  $K$ -means or Voronoi partitions (indeed, it is possible, in this case, to test whether a given edge intersects a cover element or intersection by computing the intersection of the line induced by the edge and all the mediator lines that form the boundary of the cover element). In practice, we use the largest possible  $k_n$  that still allow our estimator to be computed with a reasonable amount of time and memory usage, depending on the machine that is being used. Finally, it should be noted that small sizes of cover elements or intersections induce small  $\ell$  and large  $k_n$ , and thus potentially long computation time.

We can now state the main result, which shows that the approximation induced by our Mapper-based estimator (w.r.t. its max-bottleneck distance to the Reeb space) for probabilistic samplings follows the same rules than the standard Mapper in the deterministic case, up to a deviation term due to the sampling.

**Theorem 3.3.** *The following inequality is true:*

$$\mathbb{E} \left[ d_B^M(M_n, R_f(\mathcal{X})) \right] \leq \mathbb{E} [\text{res}(\mathcal{U})] + \mathcal{O} \left( \omega \left( \frac{\log(n)^{2/b}}{n^{1/b}} \right) \right) + \mathbb{E} \left[ \|(f - \hat{f})|_{\hat{X}_n}\|_\infty \right],$$

where  $b$  is the intrinsic dimension of  $\mathcal{X}$ .

Note that Theorem 3.3 is not completely well-defined at this point since it involves computing the max-bottleneck distance for a Mapper-based estimator computed from a finite metric space  $\hat{X}_n$ , whereas this distance can only process Mappers and Reeb spaces computed from continuous spaces (see Definition 2.6). Hence, in order to prove Theorem 3.3, we will use the so-called *Rips simplicial complex* as an intermediate object between  $\hat{X}_n$  and  $\mathcal{X}$ .

**Definition 3.4.** Let  $\hat{X}_n = \{X_1, \dots, X_n\}$  be a point cloud. The Rips simplicial complex with parameter  $\delta > 0$ , denoted by  $\text{Rips}_\delta(\hat{X}_n)$ , is the simplicial complex whose vertices are in correspondence with the points of  $\hat{X}_n$ , and such that for any  $p \in \mathbb{N}^*$  and  $\sigma = \{X_{i_1}, \dots, X_{i_p}\}$ , one has  $\sigma \in \text{Rips}_\delta(\hat{X}_n) \iff \|X_{j_1} - X_{j_2}\| \leq \delta$  for all  $j_1, j_2 \in \{i_1, \dots, i_p\}$ .

Given a Rips simplicial complex  $\text{Rips}_\delta(\hat{X}_n)$ , we also let  $\text{Rips}_\delta^1(\hat{X}_n)$  denote its 1-skeleton and  $|\text{Rips}_\delta^1(\hat{X}_n)|$  denote a geometric realization of it. Note that  $f_{\text{PL}}$  and  $\hat{f}_{\text{PL}}$  are well-defined on  $|\text{Rips}_\delta^1(\hat{X}_n)|$  by definition.

**Approximation Lemmata.** We now provide two approximation properties satisfied by the Rips complex for a point cloud  $\hat{X}_n \subseteq \mathcal{X}$  with  $n$  points (their corresponding proofs can be found in Appendix A and B). In the first one, we show that our estimator  $M_n$  is actually equivalent to the Mapper of an associated Rips complex, for which  $d_B^M$  is well-defined.

**Lemma 3.5.** The Mappers  $M_n$  and  $M_{\hat{f}_{\text{PL}}, \mathcal{U}}(|\text{Rips}_{\delta_n}^1(\hat{X}_n)|)$  are isomorphic as simplicial complexes. Hence, we define the max-bottleneck distance between  $M_n$  and  $R_f(\mathcal{X})$  as:

$$d_B^M(M_n, R_f(\mathcal{X})) = d_B^M\left(M_{\hat{f}_{\text{PL}}, \mathcal{U}}(|\text{Rips}_{\delta_n}^1(\hat{X}_n)|), R_f(\mathcal{X})\right)$$

In our second lemma, we show that the Reeb space of a space and its Rips complex approximation are actually close in the max-bottleneck distance, provided that the Rips is built on top of a dense enough point cloud.

**Lemma 3.6.** Let  $d_H^g$  denote the Hausdorff distance computed with geodesic distances on  $\mathcal{X}$ . Assume  $d_H^g(\hat{X}_n, \mathcal{X}) \leq \rho/4$  and  $\delta_n \in [4d_H^g(\hat{X}_n, \mathcal{X}), \rho]$ . Then, one has:

$$d_B^M\left(R_{\hat{f}_{\text{PL}}}(|\text{Rips}_{\delta_n}^1(\hat{X}_n)|), R_f(\mathcal{X})\right) \leq 2\omega(\delta_n) + \|(f - \hat{f})|_{\hat{X}_n}\|_\infty$$

We are now ready to prove Theorem 3.3.

*Proof.* **Theorem 3.3.** We first decompose the objective into three terms:

$$\begin{aligned} \mathbb{E} [d_B^M(M_n, R_f(\mathcal{X}))] &= \mathbb{E} \left[ d_B^M(M_{\hat{f}_{\text{PL}}, \mathcal{U}}(|\text{Rips}_{\delta_n}^1(\hat{X}_n)|), R_f(\mathcal{X})) \right] \text{ by Lemma 3.5} \\ &\leq \mathbb{E} \left[ d_B^M(M_{\hat{f}_{\text{PL}}, \mathcal{U}}(|\text{Rips}_{\delta_n}^1(\hat{X}_n)|), R_{\hat{f}_{\text{PL}}}(|\text{Rips}_{\delta_n}^1(\hat{X}_n)|)) \cdot \mathbb{I}_\Omega \right] \end{aligned} \quad (3)$$

$$+ \mathbb{E} \left[ d_B^M(R_{\hat{f}_{\text{PL}}}(|\text{Rips}_{\delta_n}^1(\hat{X}_n)|), R_f(\mathcal{X})) \cdot \mathbb{I}_\Omega \right] \quad (4)$$

$$+ \mathbb{P}(\Omega^c) \cdot D_{\mathcal{X}}, \quad (5)$$

where  $\Omega$  is the event  $\{d_H^g(\hat{X}_n, \mathcal{X}) \leq \delta_n/4\} \cap \{\delta_n \leq \rho\}$ , and  $D_{\mathcal{X}}$  is the diameter of  $\mathcal{X}$ .

Let us now bound the first two terms:

- Term (3). According to Proposition 2.7, we have

$$\mathbb{E} \left[ d_B^M(M_{\hat{f}_{\text{PL}}, \mathcal{U}}(|\text{Rips}_{\delta_n}^1(\hat{X}_n)|), R_{\hat{f}_{\text{PL}}}(|\text{Rips}_{\delta_n}^1(\hat{X}_n)|)) \cdot \mathbb{I}_\Omega \right] \leq \mathbb{E} [\text{res}(\mathcal{U})]$$

- Term (4). According to Lemma 3.6, we have:

$$\mathbb{E} \left[ d_B^M(R_{\hat{f}_{\text{PL}}}(|\text{Rips}_{\delta_n}^1(\hat{X}_n)|), R_f(\mathcal{X})) \cdot \mathbb{I}_\Omega \right] \leq 2\mathbb{E} [\omega(\delta_n)] + \mathbb{E} \left[ \|(f - \hat{f})|_{\hat{X}_n}\|_\infty \right]$$

- Term (5). Since geodesic distances are always larger than Euclidean distances, it follows that  $\mathbb{P}(\Omega^c) \leq \mathbb{P}(\Omega')$ , where  $\Omega' = \{d_H^E(\hat{X}_n, \mathcal{X}) > \delta_n/4\} \cup \{\delta_n > \rho\}$ .

We conclude by applying the inequalities  $\mathbb{E}[\omega(\delta_n)], \mathbb{P}(\Omega') \leq \mathcal{O}\left(\omega\left(\frac{\log(n)^{2/b}}{n^{1/b}}\right)\right)$ , whose proof can be found in [CMO18], Appendix A.7.  $\square$

It might not be very clear how  $\mathbb{E}[\text{res}(\mathcal{U})]$  can be controlled for a given cover algorithm. However, in a recent work [BL19], it has been shown that using a modification of  $K$ -means with the so-called *distance-to-measure*, with an algorithm that is called  $K$ -PDTM, gives a partition that can be thickened to provide a cover, and whose expected resolution can be upper bounded. More precisely, if we let  $\mathcal{Q}$  denote the partition with  $K$  cells given by  $K$ -PDTM, one has:

$$\mathbb{E}[\text{res}(\mathcal{Q}^\epsilon)] \leq \mathcal{O}\left(\frac{(\log n)^{3/2}}{\sqrt{n}} + K^{-2/d} + \epsilon\right),$$

where  $d$  is the dimension of the domain of the filter. Moreover, using the standard cover  $\mathcal{U}(r, g)$  with hypercubes leads to:

$$\mathbb{E}[\text{res}(\mathcal{U}(r, g))] = \text{res}(\mathcal{U}(r, g)) = r^d.$$

## 4 Application: Mapper in the Stochastic Filter setting

In this section, we focus on the Stochastic Filter setting, in which the filter  $\hat{f}$  used to compute the Mapper is assumed to be an estimation (computed from the data sample) of the true target filter  $f$  used to compute the Reeb space. We first provide in Section 4.1 various examples of applications of Mapper in statistics and machine learning. Indeed, standard methods provide estimated regression functions and posterior probability estimates which are interesting to study with Mapper. Then, we turn the focus to the general metric space of probability distributions in Section 4.2, and we finally provide an illustration for the metric space of combinatorial graphs with the graph edit distance in Section 4.3. Throughout the remaining of this article, the Mappers that are computed and discussed always refer to our Mapper-based estimator.

### 4.1 Stochastic Filter in Statistical Machine Learning

In this section, we discuss the various potential applications of Mappers in statistical machine learning, in which the filter is often used for inference and prediction, and we provide associated numerical experiments and illustrations. We also refer the interested reader to [HTF03] for more details on the statistical and machine learning methods used in this section.

**Stochastic real-valued filters.** We first consider the different applications in which the estimated and true target filters are real-valued functions. In this setting, our approximation result Theorem 3.3 with  $d = 1$ , or results from [CMO18], can be used to quantify the approximation and convergence of Mapper.

- **Inference.** When the target filter function only depends on the measure  $P$  itself, we can define estimators of this filter using the point cloud  $\hat{X}_n$  alone. For instance, a dimension reduction filter (e.g. PCA), the eccentricity filter or the density estimator filter are all estimators of underlying filters defined from  $P$ . See for instance [CMO18] for examples.
- **Regression.** We now assume that we observe a random variable  $Y_i$  at each point  $X_i$ :

$$Y_i = f(X_i) + \varepsilon_i, \quad i = 1, \dots, n \tag{6}$$

where the true filter is  $f(x) = \mathbb{E}(Y|X = x)$ , i.e., the regression function on  $\mathcal{X}$  and  $\varepsilon_i = Y_i - f(X_i)$ . Then, the Mapper of  $\hat{X}_n$  can be computed with any estimator  $\hat{f}$  of  $f$  (from the statistical regression literature) in order to infer the Reeb space  $R_{\hat{f}}(\mathcal{X})$ , which represents the topology of the input data through the lens of  $f$ .

- **Binary classification.** We now assume that we observe a binary variable  $Y_i \in \{-1, 1\}$  at each point  $X_i$  of the sample. Let  $f(x) = P(Y = 1|X = x)$  be the posterior probability of  $Y$  for any  $x \in \mathcal{X}$ . In this setting, inferring the target Reeb space  $R_f(\mathcal{X})$  with a Mapper computed on  $\hat{X}_n$  for some estimator  $\hat{f}$  of the posterior distribution (given by any machine learning algorithm) would provide insights about how data is topologically stratified w.r.t. the confidence given by the posterior.

**Extension to stochastic multivariate filters.** For many problems in statistical machine learning, the quantity of interest is actually a multivariate quantity. In this setting, our Mapper-based estimator can be used to control the robustness of any Reeb space inference.

- **Dimension reduction.** In this setting, a natural extension of real-valued inference described above is the projection onto the  $k$  first directions of any dimension reduction algorithm. The corresponding Mapper is now a multivariate Mapper and the underlying filter is the projection onto the  $k$  first directions of the covariance operator of  $P$ .
- **Multivariate regression.** Multivariate regression is the generalization of (univariate) regression when the variable  $Y$  in Equation (6) is now a random vector.
- **Multi-class classification.** We observe a categorical variable  $Y_i \in \{0, \dots, k\}$  at each point  $X_i$ . Let  $f_k(x) = P(Y = k|X = x)$  be the posterior probability of the class  $k$  at  $x \in \mathcal{X}$ . The underlying filter is now the vector of posterior probabilities  $f = (f_0, \dots, f_k)$ , which can be estimated with classification methods in statistical machine learning.

**Synthetic example.** We now describe two multi-class classification problems and display the corresponding Mappers. In the first one, we generate a dataset in two dimensions with three different classes which are entangled with each other. See Figure 1 (left) for an illustration. We then trained a Random Forest classifier on this dataset, and computed the estimated posterior probabilities for each of the training points, meaning that we have an estimated posterior filter  $\hat{f} : \mathbb{R}^2 \rightarrow \mathbb{R}^3$ . The corresponding Mapper (computed with 10 intervals and overlap 30% for each class) is shown in Figure 1 (right). Moreover, the Mapper nodes are colored with the variance of the posterior distributions: the larger the variance, the more confident the classifier. It is clear from the Mapper that the classifier induces a topological stratification of the data, in the sense that points in the middle of the space (located in the middle of the triangle-shaped Mapper), on which the classifier is unsure, connect with points for which the classifier hesitates between two classes (located in the middle of the "edges" of the triangle), which themselves connect with points where the classifier is confident (located at the "corners" of the triangle), leading to some non-trivial 1-dimensional topological features in the data, which are not visible at first sight on the dataset. We believe this visualization could be of great help when it comes to interpreting the output of standard statistical machine learning methods.

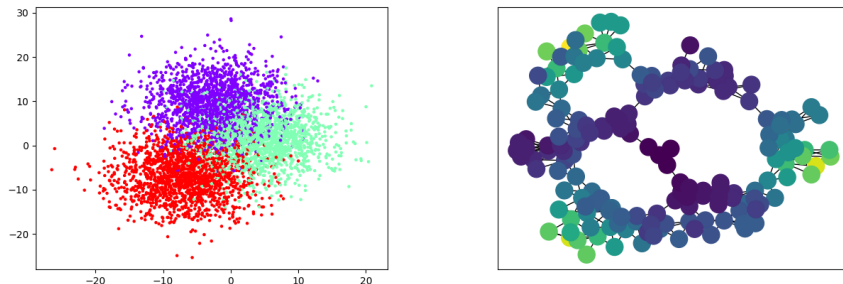


Figure 1: Three label classification problem and its corresponding Mapper. Left: we generate points in 2D with three different groups (red, purple, green). Right: Mapper computed with the posterior probability of a Random Forest classifier. Nodes are colored with the variance of the estimated probabilities from low (dark blue) to high (yellow).

**Accelerometer data.** In our second example, we study gathered time series obtained from accelerometers placed on people doing six possible types of activities, namely "standing", "sitting", "laying", "walking", "walking upstairs" and "walking downstairs". From the raw data, 561 features have been extracted on sliding window, see [AGO<sup>+</sup>13] and the data website<sup>2</sup> for more details. A Naive Bayes classifier has been trained on the 7,352 observations. We finally generated an associated Mapper with the corresponding posterior probabilities (computed with 3 intervals and 30% gain for each class), and we colored the nodes with variance, similarly to what was done above. We show the Mapper, as well as representative time series for some of its nodes, in Figure 2. Again, the classifier is inducing a topological stratification of the data, with two connected components (corresponding to the two global types of activities, namely walking activities or stationary activities), which are themselves stratified into three activities connected by time series where the classifier is unsure.

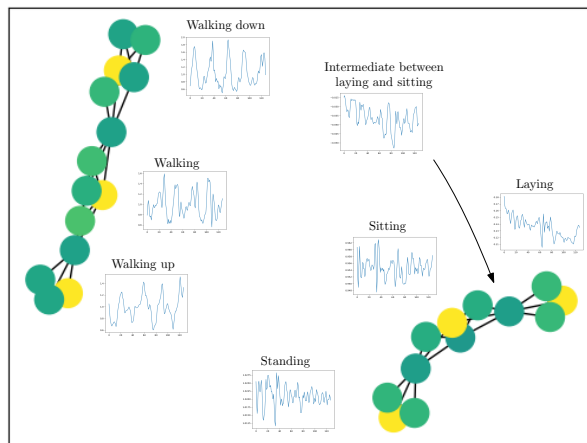


Figure 2: Mapper computed on accelerometer data with the posterior probability of a Naive Bayes classifier. Nodes are colored with the variance of the estimated probabilities from low (dark) to green (yellow).

## 4.2 Stochastic Filter with Conditional Probability Distributions

In this setting, we assume that we observe an i.i.d sample  $\{(X_i, Y_i) : 1 \leq i \leq n\}$ , where  $X_i \in \mathcal{X}$  and  $Y_i \in \mathbb{R}$  is an observation of a conditional probability distribution  $(Y|X_i)$ , which is the underlying filter value on  $X_i$ . In this framework, the filter domain is thus the space of conditional probability distributions. It might be tempting to directly compute the standard Mapper with the  $Y_i$ s as filter values. However, we recall that the target filter is actually the conditional probability distribution of  $(Y|X)$  and obviously the previous approach is not a good strategy for this aim, since single observations can be very poor estimates of the corresponding distributions.

**Mapper on probability distributions.** Let  $\mathcal{P}$  be the set of probability measures on  $\mathbb{R}$ . For  $x \in \mathcal{X}$ , let  $\nu_x$  be the conditional distribution of  $(Y|X = x)$ . Let  $\nu$  be the filter  $\nu : x \in \mathcal{X} \mapsto \nu_x \in \mathcal{P}$ . Various metrics can be proposed on  $\mathcal{P}$ , one of them being the Prokhorov metric [Bil13], which metrizes weak convergence. Generally speaking, the Reeb space  $R_\nu(\mathcal{X})$  is difficult to infer since it requires to estimate the conditional probability distribution  $\nu_x$  for all points of  $\mathcal{X}$ , which is a difficult task, especially for high dimensional data—see for instance [E<sup>+</sup>07]. As far as we know, conditional density estimation on submanifolds has not been studied yet. Moreover, as soon as  $\nu$  is injective, which is not a strong assumption in practice, the Reeb space will be isomorphic to  $\mathcal{X}$  and it will not provide more information than standard manifold learning

<sup>2</sup><https://archive.ics.uci.edu/ml/datasets/Human+Activity+Recognition+Using+Smartphones>

procedures [MF11]. We thus propose to study approximations of  $R_\nu(\mathcal{X})$ , using a filter that is a representative (such as the mean or the histogram) of  $\nu_x$ . In this situation, from a data analysis perspective, crude approximations of the Reeb space will probably show more interesting patterns than those provided by the Reeb space itself.

**Mean- and histogram-based Mappers.** Let  $\mathcal{I} = (I_1, \dots, I_k)$  be a partition of  $\mathbb{R}$  with intervals. We define the histogram filter  $\text{Hist}$  associated to  $\mathcal{I}$  by  $\text{Hist}_j(x) = P(Y \in I_j | X = x)$  for  $j = 1, \dots, k$ . The domain of  $\text{Hist}$  is in  $\mathbb{R}^k$ , i.e., it is a multivariate filter, with corresponding Reeb space  $R_{\text{Hist}}(\mathcal{X})$ . We then propose to compute the Mapper with an estimated histogram, which we call the *histogram-based Mapper*, using the Nadaraya-Watson kernel estimator:

$$\widehat{\text{Hist}}_j(x) = \frac{\sum_{i=1, \dots, n} \mathbb{I}_{Y_i \in I_j} K_h(X_i - x)}{\sum_{i=1, \dots, n} K_h(X_i - x)}$$

where  $K_h(x) = \frac{1}{h} K(\frac{x}{h})$  for a kernel function  $K$ , which we choose, in practice, to be the indicator function of the unit ball in the ambient Euclidean space. Showing an approximation result for the histogram-based Mapper can be done with Theorem 3.3, but requires to control the modulus of continuity of  $\text{Hist}$  and  $\widehat{\text{Hist}}$  on  $\mathcal{X}$ , which is beyond the scope of this paper.

Note that a simpler approach is to estimate the (conditional) mean  $f(x) = \mathbb{E}(Y|X = x)$ , and we call our corresponding estimator the *mean-based Mapper*. However, as illustrated in numerical experiments presented below, it may be not sufficient to retrieve interesting data structure.

**Numerical experiments.** We now provide examples of computations of our Mapper-based estimators computed from single realizations of synthetic conditional probability distributions<sup>3</sup>. We generate 5,000 points from an annulus, and we look at two conditional distributions for each point, namely Gaussians and bimodal ones. See Figure 3 and 4. In each of these figures, we display five Mappers: the standard Mapper, the mean-based Mapper when the true conditional mean is supposed to be known, the mean-based Mapper when this mean is estimated, the histogram-based Mapper when the true histogram is supposed to be known, and the histogram-based Mapper when the histogram is estimated. We also plot, for the standard Mapper and the mean-based Mappers, a 3D embedding of the dataset, with the mean values used as height. For the standard Mapper and the mean-based Mappers, we used an interval cover with 15 intervals and overlap percentage 30%. For the histogram-based Mapper, we used histograms with 100 bins and an 0.5-thickening of a  $K$ -PDTM cover [BL19] with  $K = 10$  cover elements.

**Gaussian conditional.** In Figure 3, we generate Gaussian conditional probability distributions centered on the second coordinates of the points. It can be seen that the standard Mapper recovers the underlying structure, but in a very imprecise way, in the sense that the feature size is much smaller than it should be, due to the variances of the distributions that induce very noisy filter values. On the other hand, the mean-based Mappers and the histogram-based Mappers all recover the correct structure in much more precise fashion.

**Bimodal conditional.** In Figure 4, we generate bimodal conditional probability distributions whose modes are centered on the second coordinate and its opposite (minus the minimum of the coordinates values). This way, all conditional probability distributions have the same mean. This time, the standard Mapper gets fooled by the probability distributions, and outputs two topological structures instead of one, due to the two modes of the distributions. The mean-based Mappers also fail due to the fact that the distributions all have the same mean, which mixes all points together and makes topological inference very difficult, leading to very noisy Mappers. On the other hand, the histogram-based Mappers both manage to retrieve the correct structure in a precise way.

### 4.3 Metric Mapper for combinatorial graphs

We end this application section by providing an example of our Mapper-based estimator, when the domain of the filter function is the space of combinatorial graphs. More specifically, we generated a graph for each

<sup>3</sup>Our code is freely available at <https://github.com/MathieuCarriere/stochmapper>

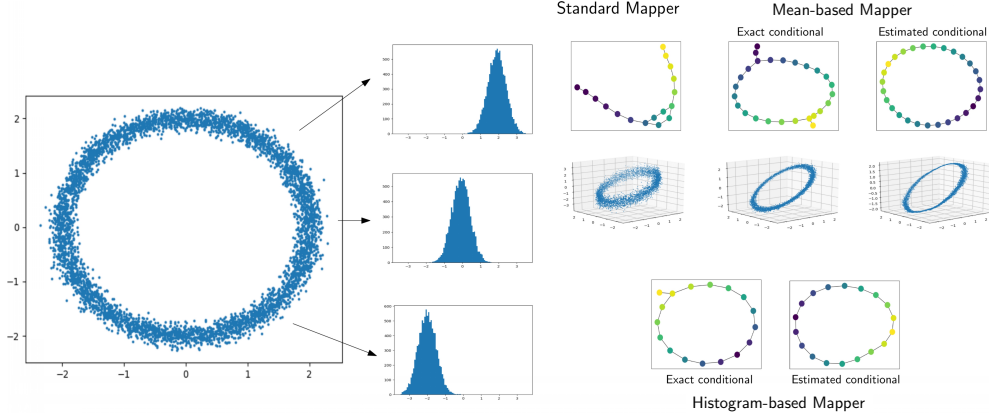


Figure 3: Standard, mean- and histogram-based Mappers computed with exact and estimated Gaussian conditional probability distributions.

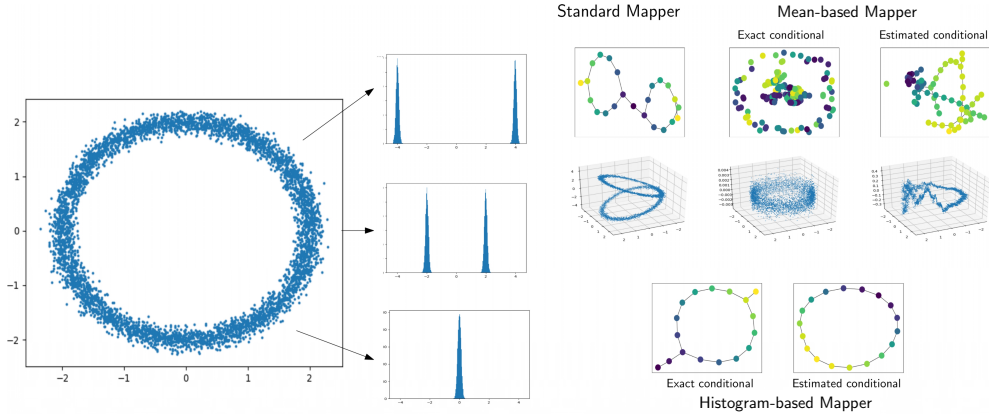


Figure 4: Standard, mean- and histogram-based Mappers computed with exact and estimated bimodal conditional probability distributions.

data point of the annulus dataset presented above, using the Erdős–Rényi model on 20 nodes, and using the first coordinate of the points (normalized between 0 and 1) as the model parameter (that is, any possible edge among the 20 nodes appears with probability given by the model parameter). This means that points located at the bottom of the annulus will have graphs with fewer edges than those above. See Figure 5 (left). Then, we used the graph edit distance [SF83] (provided in the `networkx` Python package) and a Voronoi cover with 10 cells (corresponding to 10 randomly sampled germs) and 0.5-thickening to compute our estimator. The corresponding Metric Mapper is shown in Figure 5 (right). One can see that the correct topology is retrieved by the estimator.

## 5 Conclusion and future directions

In this article, we presented a computable Mapper-based estimator that enjoys an approximation guarantee to its corresponding target Reeb space. Moreover, we demonstrated how it can be applied when the filter is estimated from a random sample of data, which we call the Stochastic Filter setting. In this case, we demonstrated a few applications in statistical machine learning, and we provided examples in which the usual Mapper fails dramatically, whereas our estimators still succeed. Much work is still needed for future directions, including demonstrating optimality and stability of the estimator. Moreover, we plan on adapting bootstrap methods to compute and interpret confidence regions. In the longer term, we also plan

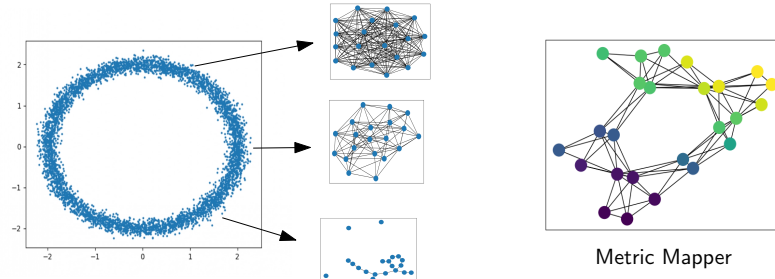


Figure 5: Example of Metric Mapper computation for combinatorial graphs.

to strengthen our results by extending them to the interleaving distance of [MW16] and to filter functions with domains included in general metric spaces.

## References

- [AGO<sup>+</sup>13] Davide Anguita, Alessandro Ghio, Luca Oneto, Xavier Parra, and Jorge Luis Reyes-Ortiz. A public domain dataset for human activity recognition using smartphones. In *Esann*, 2013.
- [BBMW19] Adam Brown, Omer Bobrowski, Elizabeth Munch, and Bei Wang. Probabilistic convergence and stability of random Mapper graphs. *arXiv*, sep 2019.
- [BGC18] Rickard Brüel-Gabrielsson and Gunnar Carlsson. Exposition and interpretation of the topology of neural networks. *arXiv*, oct 2018.
- [BGW14] Ulrich Bauer, Xiaoyin Ge, and Yusu Wang. Measuring distance between Reeb graphs. In *International Symposium on Computational Geometry*, pages 464–473, 2014.
- [Bil13] Patrick Billingsley. *Convergence of probability measures*. John Wiley & Sons, 2013.
- [BL19] Claire Bréchet and Clément Levrard. A k-points-based distance for robust geometric inference. *HAL*, 2019.
- [CdSGO16] Frédéric Chazal, Vin de Silva, Marc Glisse, and Steve Oudot. *The structure and stability of persistence modules*. Springer International Publishing, 2016.
- [CGOS11] Frédéric Chazal, Leonidas Guibas, Steve Oudot, and Primoz Skraba. Scalar field analysis over point cloud data. *Discrete & Computational Geometry*, 46(4):743–775, dec 2011.
- [CMO18] Mathieu Carrière, Bertrand Michel, and Steve Oudot. Statistical analysis and parameter selection for Mapper. *Journal of Machine Learning Research*, 19(12), 2018.
- [CO17] Mathieu Carrière and Steve Oudot. Structure and stability of the one-dimensional Mapper. *Foundations of Computational Mathematics*, 18(6):1333–1396, 2017.
- [CR19] Mathieu Carrière and Raul Rabadan. Topological data analysis of single-cell Hi-C contact maps. In *Abel Symposium*, dec 2019.
- [dSMP16] Vin de Silva, Elizabeth Munch, and Amit Patel. Categorized Reeb graphs. *Discrete & Computational Geometry*, 55(4):854–906, jun 2016.
- [E<sup>+</sup>07] Sam Efromovich et al. Conditional density estimation in a regression setting. *The Annals of Statistics*, 35(6):2504–2535, 2007.
- [GSBW11] Xiaoyin Ge, Issam Safa, Mikhail Belkin, and Yusu Wang. Data skeletonization via Reeb graphs. In *Advances in Neural Information Processing Systems*, 2011.

- [HTF03] Trevor Hastie, Robert Tibshirani, and Jerome Friedman. *The elements of statistical learning*. Springer Series in Statistics, 2003.
- [JCR<sup>+</sup>19] Rachel Jeitziner, Mathieu Carrière, Jacques Rougemont, Steve Oudot, Kathryn Hess, and Cathrin Brisken. Two-Tier Mapper, an unbiased topology-based clustering method for enhanced global gene expression analysis. *Bioinformatics*, 2019.
- [MC12] Fionn Murtagh and Pedro Contreras. Algorithms for hierarchical clustering: an overview. *Wiley Interdisciplinary Reviews: Data Mining and Knowledge Discovery*, 2(1):86–97, jan 2012.
- [MF11] Yunqian Ma and Yun Fu. *Manifold learning theory and applications*. CRC press, 2011.
- [MW16] Elizabeth Munch and Bei Wang. Convergence between categorical representations of Reeb space and Mapper. In *International Symposium on Computational Geometry*, pages 53:1–53:16, 2016.
- [NLC11] Monica Nicolau, Arnold Levine, and Gunnar Carlsson. Topology based data analysis identifies a subgroup of breast cancers with a unique mutational profile and excellent survival. *Proceedings of the National Academy of Sciences of the United States of America*, 108(17):7265–7270, apr 2011.
- [NLSKK18] Gregory Naitzat, Namita Lokare, Jorge Silva, and Ilknur Kaynar-Kabul. M-Boost: profiling and refining deep neural networks with topological data analysis. In *KDD 2018 Workshop on Interactive Data Exploration and Analytics*, 2018.
- [RCK<sup>+</sup>17] Abbas Rizvi, Pablo Cámara, Elena Kandror, Thomas Roberts, Ira Schieren, Tom Maniatis, and Raul Rabadan. Single-cell topological RNA-seq analysis reveals insights into cellular differentiation and development. *Nature Biotechnology*, 35(6):551–560, may 2017.
- [Ree46] Georges Reeb. Sur les points singuliers d’une forme de pfaff complètement intégrable ou d’une fonction numérique. *Comptes Rendus de l’Académie des Sciences de Paris*, 222:847–849, 1946.
- [SF83] Alberto Sanfeliu and King-Sun Fu. A distance measure between attributed relational graphs for pattern recognition. *IEEE Transactions on Systems, Man and Cybernetics*, 13(3):353–363, 1983.
- [SMC07] Gurjeet Singh, Facundo Mémoli, and Gunnar Carlsson. Topological methods for the analysis of high dimensional data sets and 3D object recognition. In *Eurographics Symposium on Point-Based Graphics*, pages 91–100, 2007.

## A Proof of Lemma 3.5

Let  $U_\alpha \in \mathcal{U}$ , and  $\mathcal{C}_\alpha$  be a connected component of  $\hat{f}_{\text{PL}}^{-1}(U_\alpha)$  in  $|\text{Rips}_{\delta_n}^1(\hat{X}_n)|$ . We claim that  $\mathcal{C}_\alpha \cap \tilde{X}_n \neq \emptyset$ . Indeed, if we assume that  $\mathcal{C}_\alpha \cap \tilde{X}_n = \emptyset$  then it means that  $\mathcal{C}_\alpha$  is constituted from a segment of an edge  $e$  of  $G_n$ , that does not contain the endpoints of  $e$  in  $\hat{X}_n$ , nor any points of  $\tilde{X}_n$  in the subdivision of  $e$ . Hence,  $e$  is element-crossing and  $U_\alpha$  is crossed by  $e$ . By definition, the length  $|\hat{f}_{\text{PL}}(e)|$  must be at least  $\ell = \ell(\hat{X}_n, \hat{f}, \mathcal{U})$ . Moreover, due to the subdivision process, the length  $|\hat{f}_{\text{PL}}(e)|$  must be less than  $\delta_n/(k_n + 1)$ , meaning that  $|\hat{f}_{\text{PL}}(e)|$  must be less than  $\hat{\omega}(\delta_n/(k_n + 1))$ . Hence, using the definition of  $k_n$ , we have the following inequalities:

$$\frac{\ell}{2} \geq \hat{\omega} \left( \frac{\delta_n}{\lfloor \delta_n / \hat{\omega}^{-1}(\ell/2) \rfloor + 1} \right) \geq |\hat{f}_{\text{PL}}(e)| \geq \ell,$$

which leads to a contradiction (except for  $\ell = 0$ , which happens with null probability).

Hence, for each  $U_\alpha$  and connected component  $\mathcal{C}_\alpha$  of  $\hat{f}_{\text{PL}}^{-1}(U_\alpha)$  in  $|\text{Rips}_{\delta_n}^1(\hat{X}_n)|$ , there is one point of  $\tilde{X}_n$  that belongs to  $\mathcal{C}_\alpha$ . Now, let  $\tilde{\mathcal{C}}_\alpha$  be the connected component in  $\tilde{G}_n(U_\alpha)$  (see Equation (1)) associated to this point. We now claim that  $\tilde{\mathcal{C}}_\alpha$  is included in  $\mathcal{C}_\alpha$ . Indeed, since  $\tilde{G}_n$  is nothing but a subdivision of  $|\text{Rips}_{\delta_n}^1(\hat{X}_n)|$ , and since any edge in  $\tilde{\mathcal{C}}_\alpha$  must also be present in  $\mathcal{C}_\alpha$  (otherwise it would induce an element-crossing edge in  $G_n$  whose intersection with the corresponding crossed cover element would contain no points in  $\tilde{X}_n$ , which

is impossible for the reason mentioned above), it follows that  $C_\alpha$  deform-retracts on  $\tilde{C}_\alpha$ . Hence,  $M_n$  and  $M_{f_{\text{PL}}, \mathcal{U}}(|\text{Rips}_\delta^1(\hat{X}_n)|)$  have the exact same sets of nodes.

The same argument applies straightforwardly to show that the connected components in the intersections are also in bijection, which means that the simplices of both Mappers are in correspondence as well.

## B Proof of Lemma 3.6

We first present an approximation result of Rips complexes that we use in the proof of Lemma 3.6:

**Proposition B.1** ([CGOS11]). *Let  $\mathcal{X}$  be a compact Riemannian manifold with convexity radius  $\rho$  and  $f, \hat{f} : \mathcal{X} \rightarrow \mathbb{R}$  be continuous functions on  $\mathcal{X}$ . Let  $\omega$  be the modulus of continuity of  $f$ . Let  $\hat{X}_n$  be a sampling of  $\mathcal{X}$  such that  $d_H^g(\hat{X}_n, \mathcal{X}) = \epsilon < \rho/4$  and  $4\epsilon \leq \delta \leq \rho$ , where  $d_H^g$  stands for the Hausdorff distance computed with geodesic distances on  $\mathcal{X}$ . Let  $F_\alpha = f^{-1}((-\infty, \alpha))$  and  $F_\alpha^R = \text{Rips}_\delta^1(\hat{f}^{-1}((-\infty, \alpha)) \cap \hat{X}_n)$  be the sublevel set of  $f$  and the Rips complex built on top of the points belonging to the sublevel set of  $\hat{f}$  respectively. Finally, let  $\zeta = \|(f - \hat{f})|_{\hat{X}_n}\|_\infty$ . Then the persistence modules  $\{H_0(F_\alpha)\}_{\alpha \in \mathbb{R}}$  and  $\{H_0(F_\alpha^R)\}_{\alpha \in \mathbb{R}}$  are  $\omega(\delta) + \zeta$ -interleaved.*

We can now prove Lemma 3.6. Let  $U \in \mathbf{Open}(\mathbb{R}^d)$ ,  $\alpha \in \mathbb{R}$  and  $\zeta = \|(f - \hat{f})|_{\hat{X}_n}\|_\infty$ . Let  $f^U = \|f(\cdot) - U\|$ , and

$$F_\alpha^U = (f^U)^{-1}((-\infty, \alpha)) = f^{-1}(U^\alpha),$$

and similarly, let  $\hat{f}_{\text{PL}}^U = \|\hat{f}_{\text{PL}}(\cdot) - U\|$  and

$$\hat{F}_\alpha^U = (\hat{f}_{\text{PL}}^U)^{-1}((-\infty, \alpha)) = \hat{f}_{\text{PL}}^{-1}(U^\alpha).$$

Finally, let  $F_\alpha^R = \text{Rips}_{\delta_n}^1((f^U)^{-1}((-\infty, \alpha)) \cap \hat{X}_n) = \text{Rips}_{\delta_n}^1(f^{-1}(U^\alpha) \cap \hat{X}_n)$ .

Bounding  $d_B^M$  means finding morphisms between the zeroth homology groups of  $F_\alpha^U$  and  $\hat{F}_{\alpha+\eta}^U$ , and the ones of  $\hat{F}_\alpha^U$  and  $F_{\alpha+\eta}^U$ , for some  $\eta > 0$ . Let  $\eta = \omega(\delta_n)$ . Then, since  $\omega$  is also a modulus of continuity for  $f^U$ , we can apply Proposition B.1 to  $f^U$  and  $\hat{f}_{\text{PL}}^U$  and get the following commutative diagram by combining those given by Proposition B.1:

$$\begin{array}{ccccc} H_0(F_\alpha^U) & \longrightarrow & H_0(F_{\alpha+\eta}^R) & \longrightarrow & H_0(\hat{F}_{\alpha+2\eta+\zeta}^U) \\ & \searrow & \downarrow & \searrow & \downarrow \\ & & H_0(F_{\alpha+2\eta}^U) & \longrightarrow & H_0(F_{\alpha+3\eta+2\zeta}^R) \\ & & & \searrow & \downarrow \\ & & & & H_0(F_{\alpha+4\eta+2\zeta}^U) \end{array}$$

Since one can obtain the three other diagrams (in Definition 2.6) in a similar way, this shows that  $d_B^M$  is bounded by  $2\eta + \zeta$ .